

Seismic Radiation from a Kink on an Antiplane Fault

by M. Adda-Bedia and R. Madariaga

Abstract We study radiation and energy balance for an antiplane fault containing a kink. A semi-infinite crack with a sharp rupture front propagates along the flat portion of a kinked crack. At time $t = 0$, the crack reaches the kink located at the origin of coordinates and continues propagating beyond the kink at a different speed. We compute the exact solution for this problem using a Chaplygin transformation, a variation of the well-known Cagniard–de Hoop method. We first establish an integral equation for the computation of stress intensity factor after the kink and then we solve numerically for the velocity and stress field around the crack. We find that the propagation of the crack across the kink produces a sharp change in energy balance that in turn produces a circular SH wave centered at the kink that we call the kink wave. Across the wavefront of this wave there is a sudden jump in particle velocity and radial stress. At the same time, a local stress concentration appears on the external side of the kink. We establish an exact energy balance for this problem in terms of energy rates per unit crack advance. Radiated energy is shown to maintain the balance between elastic energy released by the bulk and energy used to make the crack advance. The kink wavefront is the boundary between a field dominated by the initial flat portion of the crack and a region dominated by radiation from the kink.

Introduction

Modeling and inversion of seismic radiation from earthquakes has made substantial progress in recent years (see, e.g., Ide and Takeo [1997], Olsen *et al.* [1997], and Peyrat *et al.* [2001]). Most of these inversions use flat source models both for lack of more detailed geometrical details of the faults and in order to simplify numerical computations. Actual earthquake faults are segmented and present offsets, kinks, and bifurcations that affect seismic rupture propagation. Many authors have reported efforts to model the effect of fault geometry using different kinds of numerical methods. Some of them have studied fault kinks for mode II using numerical techniques like boundary integral equations (Kame and Yamashita, 1999, 2003; Aochi *et al.*, 2000). Three-dimensional (3D) effects were discussed by Harris and Day (1999) and Harris *et al.* (2002) using finite differences, Aochi *et al.* (2000), Aochi and Fukuyama (2002), and Aochi and Madariaga (2003) using boundary integral equations and Oglesby and Archuleta (2003), Oglesby *et al.* (2003), and Duan and Oglesby (2005) using finite elements. In an effort to understand how ruptures interact with fault kinks of arbitrary angles, Polyakov *et al.* (2002) and Kame *et al.* (2003) studied in detail the effects of kinks of different angles on in-plane (mode II) faults. In a series of experiments, Rosakis *et al.* (1999) and Rousseau and Rosakis (2003) studied ruptures propagating along flat and kinked interfaces at sub-Rayleigh and intersonic speeds. In many of these previous studies, seismic waves were computed

at particular seismic stations but, for the moment, we are not aware of any detailed study of the seismic waves radiated by a kink nor of a detailed study of energy balance when rupture interacts with the kink. In their simulation of the Izmit earthquake, Aochi and Madariaga (2003) computed the seismic-wave field radiated by several models of the fault geometry for this event. In particular, they found that geometrical discontinuities have a profound effect on rupture propagation, decreasing rupture speed and generating strong seismic-wave radiation. This has prompted us to look into more details about radiation from simple fault kinks and the waves they emit. The present model is the simplest possible example of the effect of a kink on seismic rupture. It is unlikely that the corresponding problem for mode II may be solved in such detail. Our computations may be used to guide the numerical solution of such problems and their 3D extensions.

In two previous papers, Adda-Bedia and Arias (2003) and Adda-Bedia (2004) proposed a method for determining the elastodynamic stress fields associated with the propagation of antiplane kinked or branched cracks. These authors solved the problem of a semi-infinite antiplane straight crack, initially propagating at a fixed velocity, that changes instantaneously both its direction and its rupture speed when it meets a kink on the fault. They found the explicit dependence of the stress intensity factor just after kinking as a function of the stress intensity factor before kinking, the angle of the

kink, and the instantaneous velocity of the crack tip. In the present article, we briefly present their results and then propose a solution for the velocity field around the fault with a kink. We develop a numerical method to compute the velocity and stress field radiated by the kink. These waves have a complex radiation pattern, quite different from that of dislocations, and they have a typical ω^{-2} behavior at high frequency. We derive the energy balance of the kinking process, showing that the main effect of the kink is to change the rate of energy radiation from the rupture front. Finally, an important feature of kinks is that they create weak stress concentration around the kink that reduces the available rupture energy, slowing rupture and generating wavefronts when the rupture turns the kink.

The Dynamic Kinking of an Antiplane Crack

We study the problem described in Figure 1: at time $t = 0$, a crack that has been running at constant speed v_0 along the $-x$ axis suddenly hits a kink on the fault and then continues along the kink of angle $\lambda\pi$ at a different speed v_r . As the crack runs along the horizontal axis, it has a classical

Decomposition of the kinked crack into 2 simpler problems

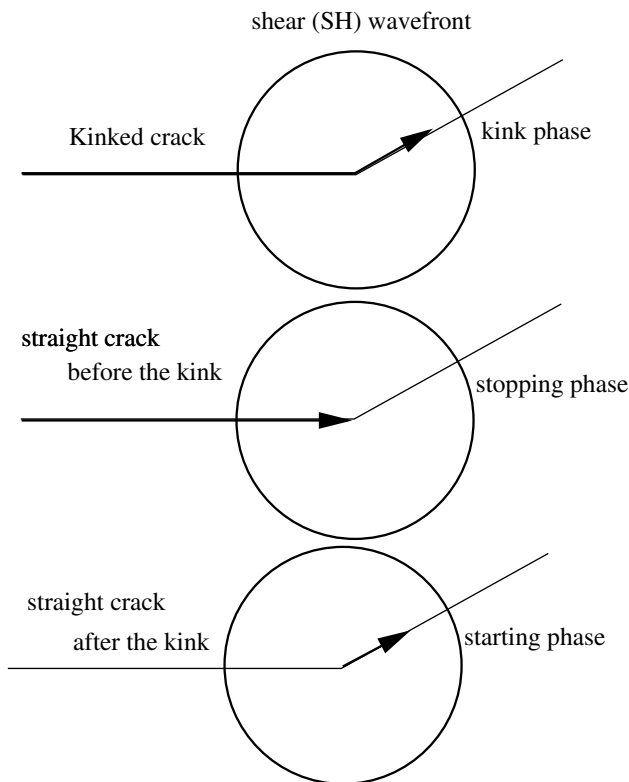


Figure 1. Geometry of the kink crack. We decompose the solution of the kinked crack problem into two simpler problems: (1) a straight crack with constant rupture speed v_0 along the negative x axis and (2) a straight crack propagating at constant speed v_r along the kink. The total radiation is the sum of the two problems. Both ruptures produce circular shear wavefronts of radius $r = \beta t$.

dynamic stress concentration K_d . When the crack moves beyond the kink, the dynamic stress intensity factor at the rupture front changes as well as its rupture speed and, simultaneously, a circular wavefront is emitted due to the change in rupture speed. Thanks to the well-known lack of inertia of cracks (Eshelby, 1969), it is possible to decompose this problem into two simpler ones (see Fig. 1): first, a crack that runs at constant speed along the negative x axis and suddenly stops at $x = 0, t = 0$. When the crack stops, the stress concentration ahead of $x = 0$ increases suddenly to K_0 and a strong stopping phase is emitted (see, e.g., Eshelby [1969] and Madariaga [1977]). At time $t = 0$, another crack suddenly starts running from $x = 0$ along the kinked path of the fault (see Fig. 1). This crack is loaded by the stress field of the previous crack and runs at a different constant speed v_r . As it starts, the second crack emits a strong starting phase with the same wavefront as the stopping phase from the first crack. The total radiation is actually the difference between the starting and stopping phases.

Propagation and Radiation by the Crack before the Kink

The radiation from the crack propagating along the first part of the fault of Figure 1b can be computed using classical crack methods. We separate the computation into two parts: the radiated field emitted by the crack propagating at constant speed and the stopping phase emitted when it suddenly stops at $x = 0$.

Let us consider the dynamic field of an antiplane crack moving at constant speed v_0 in an elastic medium of elastic rigidity μ and shear-wave speed β . The solution of this problem is very well known (see, e.g., Aki and Richards [2002]). The solution for particle velocity in moving coordinates $([x - v_0t, y])$ is

$$\dot{w}(x, y, t) = \frac{K_d}{\mu\gamma\sqrt{2\pi}} v_0 \frac{[\sqrt{(x - v_0t)^2 + \gamma^2 y^2} - (x - v_0t)]^{1/2}}{\sqrt{2}\sqrt{(x - v_0t)^2 + \gamma^2 y^2}}, \quad (1)$$

where $\gamma = \sqrt{1 - v_0^2/\beta^2}$ is the Lorentz contraction factor.

$$K_d = K_0 \sqrt{1 - v_0/\beta} \quad (2)$$

is the dynamic stress intensity factor (Freund, 1990). K_0 is the stress intensity factor that would appear at the crack tip if rupture speed v_0 suddenly dropped to zero. The velocity field (1) applies until the stopping phase from the cusp of the kink at the origin arrives to the observation point. The steady state solution (1) is like a background velocity field on top of we superpose the radiation from the kink.

Let us now study the stopping phase radiated when the crack suddenly stops at the origin. We measure time from the instant $t = 0$ when the fault stops. As shown by Eshelby (1969) and Madariaga (1977), the stopping phase produces a

sudden jump in particle velocity that drops to zero behind the *SH* wavefront. Immediately behind the stopping phase wavefront, stress and displacements take their static values. It is easier to write them in cylindrical coordinates (r, θ) centered about the origin. Defining the azimuthal and radial shear stresses,

$$\sigma_{\theta z} = \frac{\mu}{r} \frac{\partial w}{\partial \theta}, \quad \sigma_{rz} = \mu \frac{\partial w}{\partial r},$$

we find that for $r < t/\beta$,

$$\begin{aligned} \dot{w}(r, \theta) &= 0, & w(r, \theta) &= \frac{2K_0}{\mu} \sqrt{\frac{r}{2\pi}} \sin \frac{\theta}{2}, \\ \sigma_{\theta z}(r, \theta) &= \frac{K_0}{\sqrt{2\pi r}} \cos \frac{\theta}{2}, & \sigma_{rz}(r, \theta) &= \frac{K_0}{\sqrt{2\pi r}} \sin \frac{\theta}{2}. \end{aligned} \quad (3)$$

Thus, the passage of the shear wavefront leaves behind it the static stress and displacement fields of a crack of stress intensity K_0 extending along the negative x axis. This very interesting result was found by Eshelby (1969).

Propagation of the Dynamic Crack after the Kink

The process of rupture propagation beyond the kink (Fig. 1c) can be viewed as follows. For $t < 0$, it is assumed that the crack is at rest and that the material is subjected to the shear-stress field $\sigma_{\theta z}(r, \theta)$, $\sigma_{rz}(r, \theta)$ defined in equation (3).

As the crack advances for $t > 0$, displacement $w(r, \theta, t)$ satisfies the cylindrical wave equation

$$\frac{1}{r} \frac{\partial}{\partial r} \left(r \frac{\partial w}{\partial r} \right) + \frac{1}{r^2} \frac{\partial^2 w}{\partial \theta^2} = \frac{1}{\beta^2} \frac{\partial^2 w}{\partial t^2}, \quad (4)$$

with the following boundary conditions for $r \leq \beta t$:

$$\sigma_{\theta z}(r, \pm\pi, t) = 0, \quad (5)$$

$$\sigma_{\theta z}(r < v_r t, \lambda\pi \pm \epsilon, t) = 0, \quad (6)$$

$$w(\beta t, \theta, t) = \frac{2K_0}{\mu} \sqrt{\frac{\beta t}{2\pi}} \sin \frac{\theta}{2}. \quad (7)$$

Here (and elsewhere), ϵ is a vanishingly small positive constant. Boundary condition (5) states that the crack along $x < 0$ is stress free, equation (6) states that the crack along the kinked path is stress free, and the last condition (equation 7) is a consequence of the continuity of the displacement field $w(r, \theta, t)$ at the wavefront $r = \beta t$, where the following dynamic jump condition must be satisfied (see Dempsey *et al.* [1982]):

$$[\sigma_{rz}]_{r=\beta t} + \frac{\mu}{\beta} \left[\frac{\partial w}{\partial t} \right]_{r=\beta t} = 0. \quad (8)$$

To these boundary conditions, we add the regularity condition that the asymptotic behavior of the stress field near the propagating crack tip is of the form (Freund, 1990)

$$\begin{aligned} \sigma_{\theta z}(r, \lambda\pi, t) &= \left[\frac{K'}{\sqrt{2\pi(r-v_r t)}} + O(\sqrt{r-v_r t}) \right] \\ &\quad \times H(r-v_r t) \quad \text{as } r \\ &\quad \rightarrow v_r t, \end{aligned} \quad (9)$$

where H is the Heaviside function and K' is the dynamic stress intensity factor when the crack is propagating along the kink.

Self-Similar Analysis

Except for the stress intensity factor scale introduced by the boundary condition (7), there is neither a characteristic length nor a characteristic time against the independent variables r and t can be scaled. Therefore, the displacement field takes the following self-similar form

$$w(r, \theta, t) = \frac{K_0}{\mu} \sqrt{\frac{r}{2\pi}} \left[2 \sin \frac{\theta}{2} + W(s, \theta) \right], \quad (10)$$

(Adda-Bedia and Arias, 2003) where

$$s \equiv \cosh^{-1} \left(\frac{\beta t}{r} \right), \quad s \geq 0, \quad (11)$$

and W is a dimensionless function of its arguments (Miles, 1960; Achenbach, 1970; Dempsey *et al.*, 1982; Broberg, 1999).

Similarly, the stress field takes the following form

$$\sigma_{\theta z}(r, \theta, t) = \frac{K_0}{\sqrt{2\pi r}} \left[\cos \frac{\theta}{2} + S(s, \theta) \right], \quad (12)$$

with $S = \partial W / \partial \theta$, and

$$\sigma_{rz}(r, \theta, t) = \frac{K_0}{\sqrt{2\pi r}} \left[\sin \frac{\theta}{2} - \frac{\cosh s}{\sinh s} \frac{\partial W}{\partial s}(s, \theta) \right]. \quad (13)$$

Finally, taking the time derivative of equation (10), we get the particle velocity in the form

$$\dot{w}(r, \theta, t) = \frac{K_0}{\mu \sqrt{2\pi r}} v_r \frac{\cosh b}{\sinh s} \frac{\partial W}{\partial s}(s, \theta), \quad (14)$$

with $b \equiv \cosh^{-1}(\beta/v_r)$. We notice that the expressions for \dot{w} and σ_{rz} are very similar except for the factor $\cosh s$. This term is related to the singularity of stress near the origin.

In Figure 2, the transformation from the coordinate system (r, θ, t) to the (s, θ) plane is shown. Taking into account the explicit dependence of s on r and t (11) and inserting equation (10) into the wave equation (4), we find that W satisfies the partial differential equation

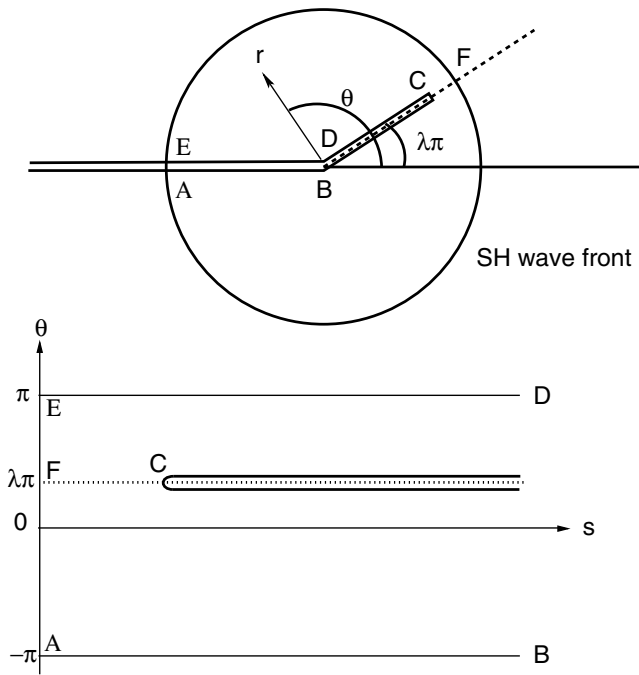


Figure 2. Geometry of the kink crack and the Chaplygin transformation from cylindrical coordinates to s and θ .

$$\frac{\partial^2 W}{\partial s^2} - \coth s \frac{\partial W}{\partial s} + \frac{\partial^2 W}{\partial \theta^2} + \frac{1}{4} W = 0. \quad (15)$$

This equation has to be solved subject to boundary conditions (5), (6), and (7), can be easily transformed into conditions on W and S . They become, respectively,

$$S(s, \pm\pi) = 0, \quad (16)$$

$$S(s > b, \lambda\pi \pm \epsilon) = -\cos \frac{\lambda\pi}{2}, \quad (17)$$

and

$$W(0, \theta) = 0. \quad (18)$$

Once the displacement field $w(r, \theta, t)$ is written under the form (10), the jump condition (8) across the cylindrical wavefront $s = 0$, corresponding to $r = ct$, is automatically satisfied.

The asymptotic behavior near the crack tip (9) imposes the following asymptotic behavior in the (s, θ) plane:

$$S(s, \lambda\pi \pm \epsilon) = -\cos \frac{\lambda\pi}{2} + \left[\frac{K'}{K_0} \frac{\sqrt{\coth b}}{\sqrt{b-s}} + O(\sqrt{b-s}) \right] \times H(b-s) \text{ as } s \rightarrow b. \quad (19)$$

Solution of the Dynamic Crack Kinking Problem

According to Adda-Bedia and Arias (2003), equation (15) admits solutions of the form

$$W(s, \theta) = \frac{2}{\pi} \int_0^s \sqrt{\cosh s - \cosh s'} \Phi(s', \theta) ds', \quad (20)$$

where $\Phi(s, \theta)$ is an unknown function that satisfies the Laplace equation in coordinates (s, θ)

$$\left[\frac{\partial^2}{\partial s^2} + \frac{\partial^2}{\partial \theta^2} \right] \Phi(s, \theta) = 0. \quad (21)$$

We can now use standard complex analysis techniques to write the solution of equation (21) as the real part of a complex function $F(\gamma = s + i\theta)$, is holomorphic inside of the contour $DCBAED$ (see Fig. 2):

$$\Phi(s, \theta) = \text{Re} [F(\gamma)] \equiv \frac{1}{2} [F(\gamma) + \overline{F(\gamma)}], \quad \gamma = s + i\theta. \quad (22)$$

The stress function S that is needed to compute tangential stress (12) can be computed from equation (20) using the Cauchy–Riemann relations. As shown by Adda-Bedia and Arias (2003),

$$S(s, \theta) = \frac{1}{\pi} \int_0^s \frac{\sinh s'}{\sqrt{\cosh s - \cosh s'}} \text{Im} [F(s', \theta)] ds'. \quad (23)$$

The transformation of the boundary conditions (16) and (20) onto conditions satisfied by F leads to

$$\text{Im} [F(s \pm i\pi)] = 0, \quad (24)$$

$$\text{Re} [F(i\theta)] = 0, \quad (25)$$

and the boundary condition (17) leads to

$$\begin{aligned} & \sqrt{\cosh s - \cosh b} \text{Im} [F(s + i\lambda\pi)] \\ &= \cos \frac{\lambda\pi}{2} - \frac{1}{\pi} \int_0^b \frac{\sqrt{\cosh b - \cosh s'}}{\cosh s - \cosh s'} \\ & \quad \times \sinh s' \text{Im} [F(s' + i\lambda\pi)] ds', \quad s > b \end{aligned} \quad (26)$$

(see Adda-Bedia and Arias [2003] for more details).

To these boundary conditions, we add the regularity conditions near the kink

$$\text{Im} [F(\gamma)] \rightarrow \sqrt{2} \exp \left[-\frac{s}{2} \right] \cos \frac{\theta}{2} \text{ as } \gamma \rightarrow \infty \quad (27)$$

and near the rupture front

$$F(\gamma) \rightarrow \frac{ia}{\gamma - \gamma_C} \text{ as } \gamma \rightarrow \gamma_C \equiv b + i\lambda\pi, \quad (28)$$

where a is a real constant, derived from equation (9), that is related to the dynamic stress intensity factor by

$$a = \frac{\sqrt{\cosh b} K'(\lambda, v_r)}{\sinh b K_0}. \quad (29)$$

The holomorphic function $F(\gamma)$ is uniquely determined by the conditions (24), (25), (26), (27), and (28). In the following, the dynamic crack kinking problem will be solved using a different method than the one used in Adda-Bedia and Arias (2003). For the present case, it is possible to get a suitable representation of the function $F(\gamma)$ without mapping it into a complex half-plane. As shown by Adda-Bedia (2004), $F(\gamma)$ can be written in a general form that satisfies the boundary conditions (24), (25), and (28),

$$F(\gamma) = a[F_1(\gamma) + F_2(\gamma)], \quad (30)$$

where $F_1(\gamma)$ and $F_2(\gamma)$ are holomorphic functions inside the contour $DCBAED$, given by

$$F_1(\gamma) = \frac{i}{2} \left[\frac{\sinh(\gamma - i\lambda\pi)/2}{\cosh(\gamma - i\lambda\pi)/2 - \cosh b/2} - \frac{\sinh(\gamma + i\lambda\pi)/2}{\cosh(\gamma + i\lambda\pi)/2 + \cosh b/2} \right], \quad (31)$$

$$F_2(\gamma) = \frac{i}{2} \int_b^\infty \left[\frac{\sinh(\gamma - i\lambda\pi)/2}{\cosh(\gamma - i\lambda\pi)/2 - \cosh t/2} - \frac{\sinh(\gamma + i\lambda\pi)/2}{\cosh(\gamma + i\lambda\pi)/2 + \cosh t/2} \right] f(t) dt, \quad (32)$$

with $f(t)$ a real continuous function defined for $t > b$. Written in the forms (31) and (32), the functions $F_1(\gamma)$ and $F_2(\gamma)$, and, consequently, $F(\gamma)$, automatically satisfy the conditions (24) and (25). Also, the condition (28) is automatically satisfied by $F(\gamma)$, through $F_1(\gamma)$. Therefore, the complete determination of the function $F(\gamma)$ is now reduced to finding the real function $f(s)$ and the real constant a . They are determined by the integral equation (26) satisfied by F (or f), combined with the additional condition (28). These can be rewritten as

$$\sqrt{2}a \cos(\lambda\pi/2) \left[\cosh b/2 + \int_b^\infty f(t) \cosh t/2 dt \right] = 1. \quad (33)$$

The function f must satisfy the integral equation (26), as shown in the Appendix can be modified into the following real-valued integral equation:

$$f(s) = A(s, b) + \int_b^\infty A(s, u) f(u) du, \quad s > b, \quad (34)$$

where the kernel $A(s, u)$ is

$$A(s, u) = \frac{1}{2\pi^2} \left[\frac{s \sinh s - u \sinh u}{\cosh s - \cosh u} - \operatorname{Re} \left(\frac{s \sinh s - (u + 2i\lambda\pi) \sinh(u + 2i\lambda\pi)}{\cosh s - \cosh(u + 2i\lambda\pi)} \right) \right]. \quad (35)$$

Let us remark that equations (34) and (35) do not involve the real constant a . Therefore, the latter integral equation can be solved independently of the value of the constant a , which can be computed from equation (33).

A complete analytical solution of the integral equation (34) cannot be derived in the general case. However, for the special case $\lambda = 0$, $A(s, u) = 0$, and $f(s) = 0$. For the general case, when $\lambda \neq 0$, the numerical resolution of the integral equation (34) can be obtained by numerical computation. In Figure 3, examples of solutions are shown for some values of λ and v_r .

Crack Front Dynamics after the Kink

The stress intensity factor just after kinking, K' , defined in equation (9), can be determined from equation (29) once the real constant a has been evaluated. Using equations (29) and (33), we find that the dynamic stress intensity factor K' is given by

$$K'(\lambda, v_r) = K_0 H_{33}(\lambda, v_r) k(v_r), \quad (36)$$

where $k(v_r) = \sqrt{1 - v_r/\beta}$, and

$$H_{33}(\lambda, v_r) = \frac{1}{\cos \lambda\pi/2 \{1 + [\int_b^\infty f(t) \cosh t/2 dt] / (\cosh b/2)\}}. \quad (37)$$

$K_0 H_{33}$ is the residual or zero-rupture velocity stress intensity factor. This is the stress intensity that would appear at the

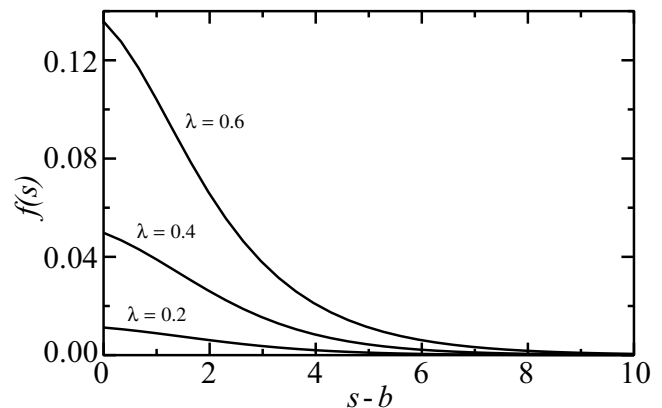


Figure 3. Plot of the function $f(s)$, solution of equation (34), for some values of the kinking angle λ and for $v_r/\beta = 0.6$.

crack tip if it were to suddenly stop. We remark that $K_0 H_{33}$ is larger than K' because the velocity dependent factor $k(v_r) \leq 1$. For $\lambda = 0$, the fault is straight and there is no change in intensity factor when the crack runs through the origin $H_{33}(0, v_r) = 1$. For angles $\lambda > 0$, we can compare H_{33} with the corresponding static results reported by Sih (1965),

$$H_{33}(\lambda, v \rightarrow 0) = \left(\frac{1 - \lambda}{1 + \lambda} \right)^{\lambda/2}. \tag{38}$$

We have computed H_{33} numerically for several values of λ and rupture velocity v_r after the kink. The corresponding results are summarized in Figure 4, where we plot $H_{33}(\lambda, v/c)$ divided by the static value (38). We observe that for small kink angles when $\lambda < 0.2$, the effect of rupture velocity is very small. At those angles we can neglect the effect of rupture speed and equation (38) becomes an excellent approximation to H_{33} .

Energy flow into the crack tip per unit crack advance, energy release rate G_c , can be computed from H_{33} ; it is

$$G_c(v_r) = \frac{K_0^2}{2\mu} H_{33}^2(\lambda, v_r) A(v_r), \tag{39}$$

where $A(v_r)$ is the universal function (Freund, 1990)

$$A(v) = \sqrt{\frac{1 - v_r/\beta}{1 + v_r/\beta}}. \tag{40}$$

Thus, as the rupture propagates along the kink, the energy release rate depends both on the intrinsic factor H_{33} and

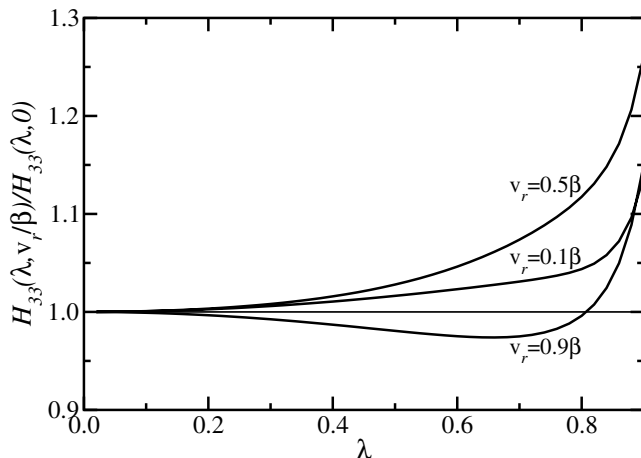


Figure 4. Plot of the function $H_{33}(\lambda, v_r/\beta)/H_{33}(\lambda, 0)$ as a function of the kinking angle and for some values of the crack tip speed just after kinking. Note that $K'(\lambda/v_r)/K_0 = \sqrt{1 - v_r/\beta} H_{33}(\lambda, v_r/\beta)$, where K' is the dynamic stress intensity factor just after kinking, and K_0 is the equilibrium stress intensity factor just before kinking. Note that for $\lambda \rightarrow 0$, H_{33} coincides exactly with the corresponding elastostatic result given by equation (38).

the rupture velocity factor $A(v_r)$, which decreases from 1 at $v_r = 0$ to 0 when $v_r = \beta$.

Seismic Waves Radiated by the Kink

We may compute full wave field produced by the rupture once we solve for the coefficient a from equation (33). Let us consider the case when the kink angle is 22.5° , that is, $\lambda = 1/8$, and the rupture speed before the kink is $v_0/\beta = 0.964$ corresponding to $b = 1.5$. We compute $F(s, \theta)$ in equation (30) numerically as a function of s and θ . Then we compute the following convolutions numerically:

$$\begin{aligned} W(s, \theta) &= \frac{2}{\pi} \int_0^s \sqrt{\cosh s - \cosh s'} \operatorname{Re} [F(s', \theta)] ds', \\ S(s, \theta) &= -\frac{1}{\pi} \int_0^s \frac{\sinh s'}{\sqrt{\cosh s - \cosh s'}} \operatorname{Im} [F(s', \theta)] ds', \\ \frac{\partial W}{\partial s}(s, \theta) &= \frac{1}{\pi} \int_0^s \frac{\sinh s}{\sqrt{\cosh s - \cosh s'}} \operatorname{Im} [F(s', \theta)] ds'. \end{aligned} \tag{41}$$

Finally, we convert then to r, θ and use equations (10), (12), (13), and (14) to compute the displacement, stresses, and velocities.

Figure 5 shows the displacement, particle velocity, and stress field $\sigma_{\theta z}$ around the origin for nondimensional time $\beta t/r = 1$, that is, the radius of the kink wavefront is 1. The slip discontinuity across the fault is materialized by the contrasting colors. The displacement field is continuous at the rupture front but is discontinuous across the kinked fault. The particle velocity field is not only discontinuous across the fault, but it presents a singularity right behind the rupture front figured by the white spot produced by the saturation of the amplitude scale.

The stress field is very interesting. We see the stress concentration at the crack tip, slightly saturated because the color scale cannot render the full range of stress values. We also observe, something that is less well known, a residual stress concentration near the origin that has the form of a horseshoe joining the kink to the rupture front. This stress concentration is positive on both sides of the fault, so that even if the fault relaxed stresses along its axis, residual stresses appear on both sides of it, preventing a complete relaxation of the stress field. This explains why speed reduces after the kink: part of the energy stored in the media cannot be completely released and it is transferred from the elastic medium surrounding the crack to the vicinity of the tip.

High Frequency Wave Radiation from the Kink

Just like the basic problem of rupture propagation across the kink was separated into two problems in Figure 1, we split high frequency waves in two parts:

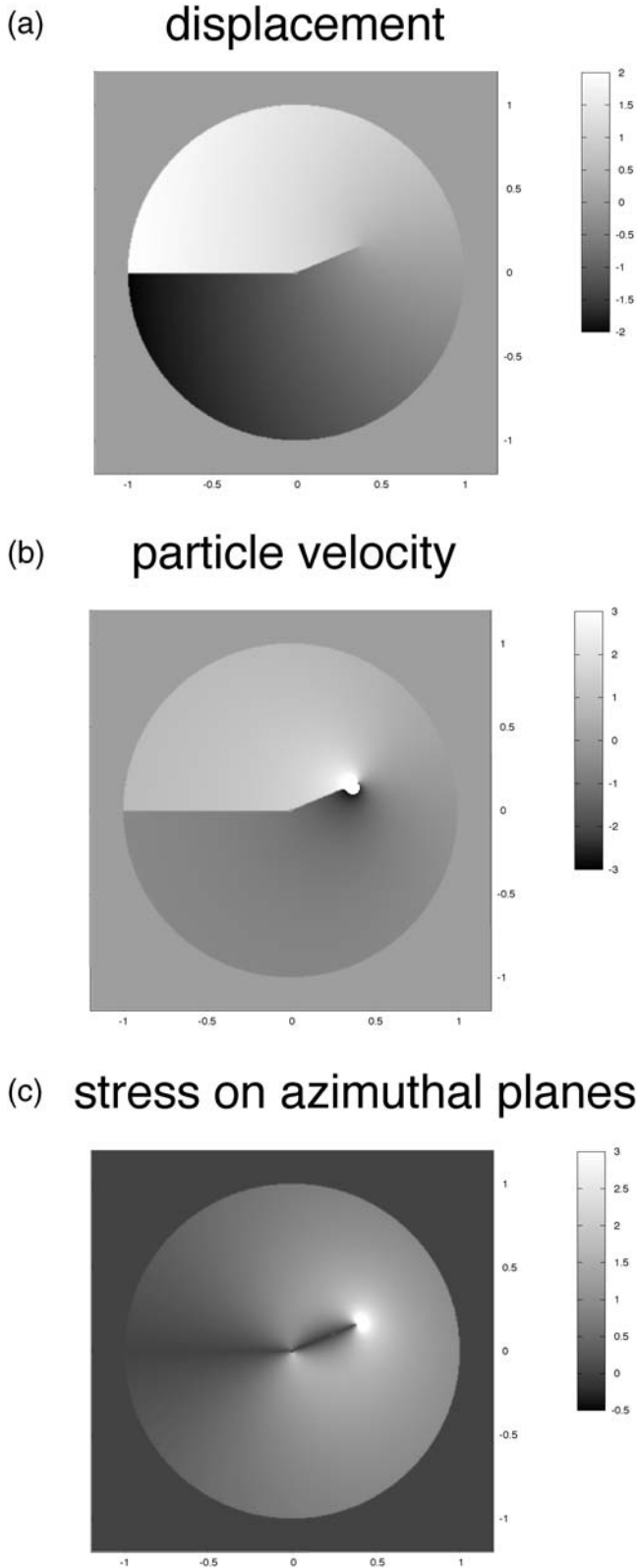


Figure 5. Plot of (a) displacement around a fault containing a kink. The displacement discontinuity is clearly shown by the color contrast across the kinked fault line. (b) Slip rate across the fault. (c) Stress $\sigma_{z\theta}$ on azimuthal planes through the origin. The computation was done for a kink angle of $\pi/8$ radians and a rupture speed parameter $b = 1.5$.

Seismic Radiation before Rupture Arrives at the Kink

When the crack propagating along the negative x axis stops at the origin, it emits a strong stopping phase that can be computed using the techniques proposed by Eshelby (1969) or Madariaga (1977). Across the wavefront $r = \beta t$, particle velocity experiences a sudden jump of amplitude:

$$\dot{w}(r, \theta, t) = -\frac{K_0}{\mu\sqrt{2\pi r}} v_0 \frac{\sin \theta/2}{1 - (v_0/\beta) \cos \theta} H(t - r/\beta). \quad (42)$$

Seismic Radiation after the Rupture Leaves the Kink

When rupture starts moving along the kink it also emits a strong wave that we can compute once we find $F(\gamma)$. Inserting equation (20) into the particle velocity function (14), we get

$$\dot{w}(r, \theta, t) = \frac{K_0}{\mu\sqrt{2\pi r}} v_r \cosh b \int_0^s \frac{\text{Re}[F(s', \theta)]}{\sqrt{\cosh s - \cosh s'}} \frac{ds'}{\pi}. \quad (43)$$

We are interested in the particle velocity when approaching the wavefront $r = \beta t$, or equivalently $s = 0$. In this limit it is seen that the contribution to the integral in equation (43) is nonzero for $s' \approx s \approx 0$ only. Using $\cosh s \approx 1 + s^2/2$ and performing the variable change $s' = sx$, we can integrate equation (43) exactly to

$$\dot{w}(r, \theta, t) = \frac{K_0}{\mu\sqrt{2\pi r}} v_r \frac{\cosh b}{\sqrt{2}} \text{Re}[F(0, \theta)] H(t - r/\beta). \quad (44)$$

Once the analytic function F is determined, we can calculate this quantity. It can be easily verified that for $\lambda = 0$ one recovers the exact known result (Eshelby, 1969):

$$\dot{w}(r, \theta, t) = \frac{K_0}{\mu\sqrt{2\pi r}} v_r \frac{\sin \theta/2}{1 - (v_r/\beta) \cos \theta} H(t - r/\beta), \quad (45)$$

which, as expected, has the same form as the stopping phase when the initial crack stops at the origin. If there is no rupture speed jump, that is, if $v_r = v_0$, then the starting phase (45) exactly cancels the stopping phase (42).

We observe from equation (44) that radiated waves decay like $r^{-1/2}$ in the far field, just like the velocity field behind the rupture front. The similarity of the behavior of velocity concentration and far-field radiation is a unique property of the 2D crack radiation.

It is not difficult to show that, as expected, displacement w and the tangential stress $\sigma_{z\theta}$ are continuous at the rupture front. Radial stress σ_{zr} , on the other hand, is discontinuous at the kink wavefront, just like \dot{w} . Actually the jump in stress is just $\sigma_{rz} = \rho\beta\dot{w}$, where $\rho\beta$ is the impedance of the bulk.

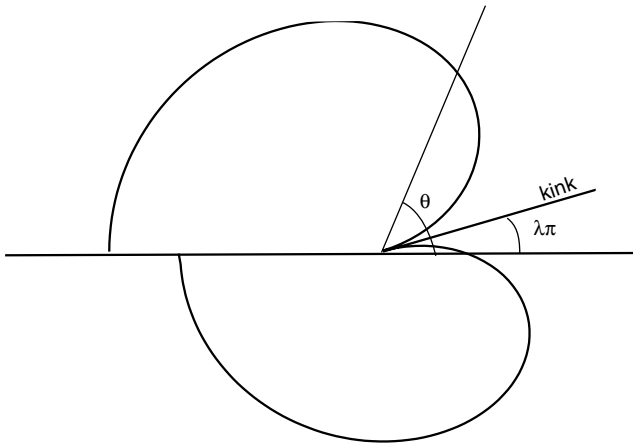


Figure 6. Radiation pattern of the kink wave, the velocity discontinuity emitted by the kink when ruptures cross the origin. This wave has a jump in particle velocity whose amplitude is shown in the figure. We notice that the nodal line does not coincide with the direction of the kink.

In Figure 6, we compute radiation pattern for different angles λ . We observe that the nodal line of the radiation pattern is not aligned with the kink direction but is intermediate between the $x = 0$ line and the direction of the kink.

We can now compute the high frequency asymptote of spectral amplitude of the displacement field associated with the particle velocity jump described by equation (44). Taking Fourier transform, we find

$$\tilde{w}(r, \theta, \omega) = \frac{K_0}{\mu\sqrt{2\pi r}} v_r \frac{\cosh b}{\sqrt{2}} \operatorname{Re} [F(0, \theta)] \frac{1}{\omega^2} e^{-i\omega r/\beta}. \tag{46}$$

We observe that the kink wave has a typical ω^{-2} high frequency behavior. Thus, radiation from a kink behaves just like the stopping phases from flat cracks studied by Madariaga (1977).

Stress Concentration near the Kink

We have already mentioned that stress near the tip of the kink has a particular decay with distance from the kink r and with the angle θ . The residual stresses around the kink, once the crack has moved far enough from it, is controlled by the state of stress of a wedge with free boundary conditions (Achenbach, 1970). We study this state of stress because it plays an important role in the energy balance of the kink. Following Achenbach, we introduce a general solution of the Laplace equation in polar coordinates:

$$w(r, \theta) = Ar^p \cos(p\theta + \phi), \tag{47}$$

where A and ϕ are the phase and amplitude to be determined. The tangential shear stress associated with this solution is

$$\sigma_{\theta z}(r, \theta) = -Apr^{p-1} \sin(p\theta + \phi) \tag{48}$$

Once the crack has propagated away from the kink, the two sides of the kink are free to slip so that

$$\sigma_{\theta z}(r, -\pi) = 0, \tag{49}$$

$$\sigma_{\theta z}[r, (1 \pm \lambda)\pi] = 0, \tag{50}$$

where the angle of the kink is $(1 + \lambda)\pi$ on the external side of the kink and $(1 - \lambda)\pi$ on the internal one.

The first condition in equation (49) is satisfied if $\phi = \pi$; the second one requires that

$$\sin[p(1 \pm \lambda)\pi + \pi] = 0. \tag{51}$$

This defines a many-valued eigenvalue problem for p . In our problem, we are interested in the most singular eigenvalues, $p = 1/(1 \pm \lambda)$.

Inserting these values of p into equations (47) and (48), we get the full solution compatible with free boundary conditions on the fault. We observe, however, that the stress fields on the two sides of the kink behave differently. Let us consider the external side first. On this side, $-\pi < \theta < \lambda\pi$, we get

$$w(r, \theta) = Ar^{1/(1+\lambda)} \cos \frac{\pi + \theta}{1 + \lambda}, \tag{52}$$

$$\sigma_{\theta z}(r, \theta) = -Apr^{-\lambda/(1+\lambda)} \sin \frac{\pi + \theta}{1 + \lambda}, \tag{53}$$

and stresses increase like $r^{-\lambda/(1+\lambda)}$ near $r = 0$. For $0 < \lambda < 1/2$, the power decreases from 0 to $-1/3$. This is a weak singularity of lower order than typical crack singularities, which have a power of $-1/2$.

On the internal side, $\pi < \theta < \lambda\pi$, we get

$$w(r, \theta) = Ar^{1/(1-\lambda)} \cos \frac{\pi - \theta}{1 - \lambda}, \tag{54}$$

$$\sigma_{\theta z}(r, \theta) = -Apr^{\lambda/(1-\lambda)} \sin \frac{\pi - \theta}{1 - \lambda}, \tag{55}$$

so that stresses behave like $r^{\lambda/(1-\lambda)}$, which increases from 0 at $\lambda = 0$ to 1 for $\lambda = 1/2$. Stresses in the internal side of the kink behave regularly; actually, they increase away from it as observed in Figure 5c. These results fully agree with those presented by Achenbach (1970). We observe from the solution (52) that displacement at the corner of the kink is continuous and presents weak discontinuities of order $1/(1 \pm \lambda)$. Because we are interested in kinks with small angles, such that $\lambda < 1/2$, $p > 1$, w is continuous at the origin and has a weak first order discontinuity with a power larger than $2/3$.

Energy Balance

Seismic energy has been the subject of much recent discussion because it is widely used to determine the overall energy balance of earthquakes (see Ide and Takeo [1997], Madariaga and Olsen [2000], Favreau and Archuleta [2003], and Rivera and Kanamori [2005]). Energy balance can be completely solved for the present model, which we hope will help in understanding the detailed energy balance for this particular example. Energy balance for earthquake sources was studied by Kostrov (1974) and Husseini *et al.* (1975), producing several equivalent expressions that have created some confusion. In the present problem by construction stress falls to zero (or a residual but uniform level everywhere on the fault behind the rupture front). Thus, in this case the energy balance is much simpler than that derived by Kostrov.

Because our fault model is actually infinite, the energy balance can only be written in the form of energy flow per unit crack advance. Let us first compute the energy per unit crack advance emitted by a crack running at constant rupture speed v_r along the flat part of the fault. Let us consider a point on the fault. The velocity field produced by the passage of the rupture front through this point is (see Madariaga [1983])

$$\dot{w}(r, \theta, t) = \frac{K_d}{\mu\sqrt{2\pi r}} v_r \frac{\sin \theta/2}{1 - (v_r/\beta) \cos \theta} H(t - r/\beta), \quad (56)$$

where r, θ refer to cylindrical coordinates drawn around the reference point. We consider the energy flow across a circle of fixed radius r around this point. The energy per unit time and unit solid angle that flows across this circle is

$$\frac{\partial E_s}{\partial t} r d\theta = \sigma_{rz} \dot{w}_z r d\theta. \quad (57)$$

In the far field, $\sigma_{rz} = \rho\beta\dot{w}$, and because we are interested in the amount of energy radiated per unit crack advance,

$$\begin{aligned} \frac{\partial E_s}{\partial x} &= \int_0^{2\pi} \rho\beta\dot{w}^2 \frac{dt}{dx} r d\theta \\ &= \frac{K_d^2 v_r}{\mu \beta \pi} \int_0^{2\pi} \frac{\sin^2 \theta/2}{1 - (v_r/\beta) \cos \theta} d\theta, \end{aligned}$$

where we used the derivative $dt/dx = 1/v_r[1 - (v_r/\beta) \cos \theta]$ that relates travel-time change dt to rupture front advance dx , as shown in Figure 7. We can now do the integration over θ exactly. Using integration tables:

$$e_s = \frac{\partial E_s}{\partial x} = \frac{K_0^2}{2\mu} \left[1 - \sqrt{\frac{1 - v_r/\beta}{1 + v_r/\beta}} \right], \quad (58)$$

where we used the classical notation that energy density is represented by a lower case letter. In equation (58), we have split K_d into the product of the static stress intensity factor

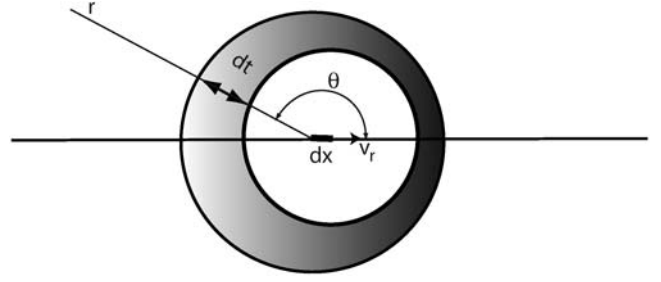


Figure 7. Computation of the radiated energy flow per unit advance of a crack front. The energy radiated when the crack advances by a distance dx is contained in the shaded area of the figure, between the circular wavefront emitted from the beginning of the segment dx and the wavefront emitted from the end of the segment. The time difference between the arrival of the two fronts is a function of the radiation angle; it has the same form as the well-known directivity effects of rupture propagation.

K_0 and the universal velocity factor $k(v_r) = \sqrt{1 - v_r/\beta}$ (see equation 2).

Equation (58) can be compared now to that proposed by Husseini *et al.* (1975) and Freund (1990). In our notation,

$$e_s(x) = \Delta e_w(x) - G_c(v_r, x), \quad (59)$$

where Δe_w is the elastic energy released by the bulk for unit crack advance and G_c is the energy release rate, the energy used to advance the crack front a unit distance. When the crack advances quasistatically at speed $v_r \rightarrow 0$, there is no energy radiation, so that

$$\Delta e_w(x) = G_c(0, x). \quad (60)$$

Now, we use the property that $G_c(v_r) = A(v_r)G_c(0)$, where $A(v_r)$ is the universal function defined in equation (40) that relates energy release rate at different rupture speeds and $G_c(0) = K_0^2/2\mu$. Thus, the seismic energy density radiated from point x along the crack is

$$e_s(x) = [1 - A(v_r)] \frac{K_0^2}{2\mu} = [1 - A(v_r)] G_c(0). \quad (61)$$

This result is valid whatever the rupture speed is along the crack. It simply says that the local seismic efficiency, that is, the ratio of elastic energy radiated to the amount of energy released, is just

$$\eta = \frac{e_s}{\Delta e_w} = 1 - A(v_r) \quad (62)$$

and that the rupture control parameter κ is

$$\kappa = \frac{\Delta e_w}{G_c(v_r)} = \frac{1}{A(v_r)}. \quad (63)$$

As expected, rupture velocity is determined by κ (see Madariaga and Olsen [2000] for a more extensive discussion).

The energy balance (59) was established for a crack running along the flat part of the kink. Once the crack has moved beyond the kink, a similar calculation could be used to determine energy balance. It is much simpler here to use the relations from Husseini *et al.* (1975) to do this calculation.

We can now apply the energy balance to our model of the kink. Before the crack reaches the kink, it emits seismic-wave energy at a rate given by

$$e_s^0 = [1 - A(v_0)] \frac{K_0^2}{2\mu}, \tag{64}$$

and once it moves into the kink, the radiated energy per unit crack advance changes to

$$e_s^1 = [1 - A(v_r)] \frac{K_0^2 H_{33}^2(\lambda, v_r)}{2\mu}, \tag{65}$$

where H_{33} was computed earlier (39). It is important to realize that the radiated energy after the kink is not determined only by the factor $[1 - A(v_r)]$ as in flat cracks but also by a factor H_{33} that depends on rupture and angle. It is only for small rupture speeds that we expect that H_{33} becomes independent of rupture speed.

The process of energy radiation from a kinked fault is illustrated in Figure 8. As the crack propagates at constant speed, before and after the kink, it emits a constant amount of seismic energy per unit crack advance defined by equation (64) before the kink and equation (65) after the kink. The kink wave produced when the rupture front hits the corner of the kink does not carry a finite amount of energy. It actually represents a sudden jump in the amount of seismic energy radiated by the fault. It is interesting to remark that contrary to more complex models of faulting our model permits a detailed local energy flow balance. We can clearly identify how the strain energy released from the medium

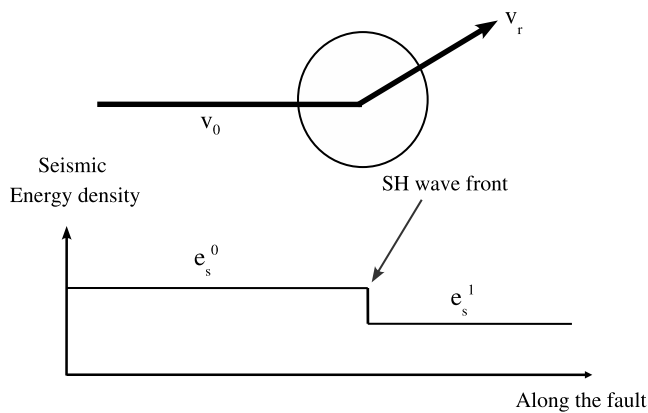


Figure 8. Variation of radiated energy flux as a function of position along the fault. Before and after the kink, the fault generates a constant amount of energy flux, noted e_s^0 and e_s^1 . High frequency radiation occurs at the kink because energy flow changes abruptly in response to the sudden change of direction of the fault.

can be split into energy release rate and radiated seismic energy. In our simple model, where rupture speed is completely determined, the ratio of radiated energy to energy release rate is entirely determined by the local rupture velocity. This is an apparent violation of Rivera and Kanamori (2005), but their statement concerned total radiated energy, not energy flow as we show here.

Discussion and Conclusions

Using a method developed by Adda-Bedia and Arias (2003) and Adda-Bedia (2004), the stress and particle velocity fields generated by the propagation of an antiplane kinked crack have been determined. In the earlier paper, the complex function $F(\gamma)$ in equation (30) was found by mapping of the function F to a certain complex plane that was difficult to find and prone to error. In the present article, $F(\gamma)$ was found using symmetry properties of the solution and the boundary conditions in the complex plane γ . With this approach, we found a complete solution of the problem that can be computed numerically. From the solution, we computed the dynamic stress intensity factor right after kinking as a function of the stress intensity factor just before kinking, the angle of the kink, and the instantaneous velocity of the crack tip.

From a seismological point of view, the seismic wave radiated when the rupture front turns at the kink could be computed numerically. This generates a strong seismic wave that we have called the kink wave. Across the wavefront, the kink wave produces a jump in particle velocity that can be computed exactly. This jump in particle velocity corresponds in the spectral domain to a high frequency decay of type ω^{-2} as in most earthquakes. This model can thus be used to build more general models of velocity change phases for nonplanar faults.

Studying the far-field radiation from a moving crack, we could compute the seismic energy radiation per unit crack advance and we could establish a complete energy balance per unit crack propagation distance. This balance states that the amount of potential energy released from the bulk per unit crack advance is equal to the sum of the energy radiated and the energy released to the rupture front. Rupture propagation is thus controlled by the balance between energy release and energy radiated by seismic waves. This simple balance equation can be derived from earlier work by Husseini *et al.* (1975), but in most seismological applications, authors have looked for global rather than a local energy balance as we do here.

Finally, we showed that weak stress concentrations are generated near the kinks that play an interesting role in the redistribution of energy during seismic ruptures. These stress concentrations may be the sites of possible aftershocks located close to a broken fault as suggested by J. Dieterich (personal comm., 2005). In this sense, the rupture of a kinked fault is mechanically much more interesting than a flat fault where all of the energy released from the bulk is used to propagate the rupture and produce seismic waves. In the pre-

sence of kinks, a fraction of the energy that flows into the fault is used to produce residual stress concentrations located close to the kink points. These weak stress concentrations may be the sites of aftershocks,

The results presented here were for the antiplane mode of faulting; in this mode, slip occurs in the direction perpendicular to the fault section so that there are no incompatibilities at the corner of the kink. It is very unlikely that similar closed form solutions may be found for the in-plane mode, because in this case the behavior of the corner point must be explicitly defined because the normal to the fault plane is ambiguous at this point. In spite of this difference, we anticipate that several properties of our solution will prevail. The main feature we expect to remain valid is that the stress intensity factor will suddenly change when the rupture starts to propagate into the kink; this will generate seismic body waves characterized by jumps in particle velocity. A feature that will be quite different is that surface waves will be generated along the fault and the kink. Numerical results have been published for mode II kinks, but they are difficult to interpret because the boundary conditions at the corner of the kink were not always explicitly posed. As we mentioned previously, the normal to the fault is not defined at the corner, so the mechanical problem of the kink in mode II or I is ill posed. It needs additional assumptions about the geometry of the corner of the kink, as discussed by Tada and Yamashita (1996). For 3D problems, the wavefronts can be computed using ray methods as discussed by Madariaga (1977) and Bernard and Madariaga (1984). Unfortunately, the amplitudes of the kink waves and their radiation patterns cannot be computed unless the mode II problem can be solved, because these solutions are needed as canonical problems.

Data and Resources

No data were used in this article. Some plots were prepared using the gnuplot program available from <http://www.gnuplot.info/>.

Acknowledgments

Laboratoire de Physique Statistique de l'École Normale Supérieure is associated with Centre National de la Recherche Scientifique (CNRS) (UMR 8550) and with Universities Paris VI and Paris VII. Raul Madariaga's work was supported by the SPICE Research and training network of the European Community.

References

- Achenbach, J. D. (1970). Shear waves in an elastic wedge, *Int. J. Solids Struct.* **6**, 379–388.
- Adda-Bedia, M. (2004). Brittle fracture dynamics with arbitrary paths—II. Dynamic crack branching under general antiplane loading, *J. Mech. Phys. Solids* **52**, 1407–1420.
- Adda-Bedia, M., and R. Arias (2003). Brittle fracture dynamics with arbitrary paths—I. Dynamic crack kinking under general antiplane loading, *J. Mech. Phys. Solids* **51**, 1287–1304.
- Aki, K., and P. G. Richards (2002). *Quantitative Seismology*, Second Ed., University Science Books, Sausalito, California.
- Aochi, H., and E. Fukuyama (2002). Three dimensional non-planar simulations of the Landers earthquake, *J. Geophys. Res.* **107**, 2035, doi 10.1029/2000JB000061.
- Aochi, H., and R. Madariaga (2003). The 1999 Izmit, Turkey, earthquake: non-planar fault structure, dynamic rupture process, and strong ground motion, *Bull. Seismol. Soc. Am.* **93**, 1249–1266.
- Aochi, H., E. Fukuyama, and M. Matsu'ura (2000). Spontaneous rupture propagation on a non-planar fault in 3-D elastic medium, *Pure Appl. Geophys.* **157**, 2003–2027.
- Bernard, P., and R. Madariaga (1984). High frequency seismic radiation from a buried circular fault, *Geophys. J. R. Astr. Soc.* **78**, 1–18.
- Broberg, K. B. (1999). *Cracks and Fracture*, Academic, New York.
- Dempsey, J. P., M. K. Kuo, and J. D. Achenbach (1982). Mode III kinking under stress wave loading, *Wave Motion* **4**, 181–190.
- Duan, B., and D. D. Oglesby (2005). Multicycle dynamics of nonplanar strike-slip faults, *J. Geophys. Res.* **110**, B03304, doi 10.1029/2004JB003298.
- Eshelby, J. D. (1969). The elastic field of a crack extending nonuniformly under general antiplane loading, *J. Mech. Phys. Solids* **17**, 177–199.
- Favreau, P., and R. J. Archuleta (2003). Direct seismic energy modelling and application to the 1979 Imperial Valley earthquake, *Geophys. Res. Lett.* **30**, 1198, doi 10.1029/2002GL015968.
- Freund, L. B. (1990). *Dynamic Fracture Mechanics*, Cambridge University Press, New York.
- Harris, R. A., and S. Day (1999). Dynamic 3D simulations of earthquakes on en echelon faults, *Geophys. Res. Lett.* **26**, 2089–2092.
- Harris, R. A., J. F. Dolan, R. Hartleb, and S. M. Day (2002). The 1999 Izmit, Turkey earthquake: a 3D dynamic stress transfer model of intraeathquake triggering, *Bull. Seismol. Soc. Am.* **92**, 245–255.
- Husseini, M. I., D. B. Jovanovich, M. J. Randall, and L. B. Freund (1975). The fracture energy of earthquakes, *Geophys. J. R. Astr. Soc.* **43**, 367–385.
- Ide, S., and M. Takeo (1997). Determination of constitutive relations of fault slip based on seismic wave analysis, *J. Geophys. Res.* **102**, 27,239–27,391.
- Kame, N., and T. Yamashita (1999). Simulations of the spontaneous growth of a dynamic crack without constraints on the crack tip path, *Geophys. J. Int.* **130**, 345–358.
- Kame, N., and T. Yamashita (2003). Dynamic branching, arresting of rupture and the seismic wave radiation in self-chosen crack path modelling, *Geophys. J. Int.* **155**, 1042–1050.
- Kame, N., J. R. Rice, and R. Dmowska (2003). Effects of prestress state and rupture velocity on dynamic fault branching, *J. Geophys. Res.* **108**, 2265, doi 10.1029/2002JB002189.
- Kostrov, B. V. (1974). Seismic moment and energy of earthquakes and seismic flow of rocks, *Izvestia: Earth Phys.* **1**, 23–40.
- Madariaga, R. (1977). High frequency radiation from crack (stress drop) models of earthquake faulting, *Geophys. J. R. Astr. Soc.* **51**, 525–651.
- Madariaga, R. (1983). High frequency radiation from dynamic earthquake fault models, *Ann. Geophys.* **1**, 17–23.
- Madariaga, R., and K. B. Olsen (2000). Criticality of rupture dynamics in 3D, *Pure Appl. Geophys.* **157**, 1959–1979.
- Miles, J. W. (1960). Homogeneous solutions in elastic wave propagation, *Quart. Appl. Math.* **18**, 37–59.
- Muskhelishvili, N. I. (1953). *Singular Integral Equations*, Noordhoff, Groningen.
- Oglesby, D. D., and R. J. Archuleta (2003). The three-dimensional dynamics of a non-planar thrust fault, *Bull. Seismol. Soc. Am.* **93**, 2222–2235.
- Oglesby, D. D., S. M. Day, Y-G LI, and J. E. Vidale (2003). The 1999 Hector Mine earthquake: the dynamics of a branched fault system, *Bull. Seismol. Soc. Am.* **93**, 2459–2476.
- Olsen, K. B., R. Madariaga, and R. J. Archuleta (1997). Three-dimensional dynamic simulation of the 1992 Landers earthquake, *Science* **278**, 834–838.
- Peyrat, S., K. B. Olsen, and R. Madariaga (2001). Dynamic inversion of the Landers earthquake, *J. Geophys. Res.* **106**, 25,467–25,482.

- Poliakov, A., R. Dmowska, and J. R. Rice (2002). Dynamic shear rupture interactions with fault bends and off-axis secondary faulting, *J. Geophys. Res.* **107**, 2295, doi 10.1029/2001JB000572.
- Rivera, L., and H. Kanamori (2005). Representations of the radiated energy in earthquakes, *Geophys. J. Int.* **162**, 48–155.
- Rosakis, A. J., O. Samudrala, and D. Coker (1999). Cracks faster than the shear wave speed, *Science* **284**, 1337–1340.
- Rousseau, C. E., and A. J. Rosakis (2003). On the influence of fault bends on the growth of sub-Rayleigh and intersonic dynamic shear ruptures, *J. Geophys. Res.* **108**, 2411, doi 10.1029/2002JB002310.
- Sih, G. C. (1965). Stress distribution near internal crack tips for longitudinal shear problems, *J. Appl. Mech.* **32**, 51–58.
- Tada, T., and T. Yamashita (1996). The paradox of smooth and abrupt bends in two-dimensional in-plane shear-crack mechanics, *Geophys. J. Int.* **127**, 795–800.

Appendix

In the following, we focus on the transformation of the integral equation (26) into equation (34). Using the representations (31) and (32), it is shown that

$$\text{Im} [F(s + i\lambda\pi)] = \frac{a}{2} \left[I(s, b) + \int_b^\infty I(s, t) f(t) dt \right], \quad (\text{A1})$$

$$I(s, t) = \text{Re} \left[\frac{\sinh(s/2)}{\cosh(s/2) - \cosh(t/2)} - \frac{\sinh[(s + 2i\lambda\pi)/2]}{\cosh[(s + 2i\lambda\pi)/2] + \cosh(t/2)} \right]. \quad (\text{A2})$$

Equation (A2) can be easily transformed into

$$I(s, t) = I_1(s, t) + I_2(s, t), \quad (\text{A3})$$

where

$$I_1(s, t) = \frac{4 \cosh(t/2) \sinh(s/2)}{\cosh(s) - \cosh(t)}, \quad (\text{A4})$$

$$I_2(s, t) = \frac{\sinh(s/2)}{\cosh(s/2) + \cosh(t/2)} - \text{Re} \left[\frac{\sinh(s/2)}{\cosh(s/2) + \cosh[(t + 2i\lambda\pi)/2]} \right]. \quad (\text{A5})$$

Using equations (A1), (A4), and (A5), the integration over s' in equation (26) can be computed analytically. For this, we need to analytically calculate integrals of the following types

$$J_1(z) = \int_1^b \frac{\sqrt{(b-x)(x-1)} dx}{x-z} \frac{1}{\pi} = \sqrt{(z-b)(z-1)} - z + (b+1)/2. \quad (\text{A6})$$

After some algebraic manipulation and using equation (33), an integral equation satisfied by the real function f is deduced. It is given by

$$\int_b^\infty \frac{\sqrt{\cosh(t) - \cosh(b)}}{\cosh(t) - \cosh(s)} f(t) \sinh(t) dt = \frac{\sin^2(\lambda\pi/2)}{a \cos(\lambda\pi/2)} + H(s, b) + \int_b^\infty H(s, t) f(t) dt, \quad (\text{A7})$$

$$H(s, t) = \frac{1}{2} \sqrt{\cosh(s) - \cosh(b)} I_2(s, t) - \int_0^b \frac{\sqrt{\cosh(b) - \cosh(s')}}{\cosh(s') - \cosh(s)} I_2(s', t) \sinh(s') \frac{ds'}{2\pi}, \quad (\text{A8})$$

where the integral in the left-hand side of equation (A7) must be taken in the sense of Cauchy principal value. One can write equation (A7) differently by noticing that it is in the form of a Hilbert singular integral equation. Thus, one can invert it to obtain (Muskhelishvili, 2003)

$$f(s) = A(s, b) + \int_b^\infty A(s, u) f(u) du, \quad s > b, \quad (\text{A9})$$

$$A(s, u) = - \int_b^\infty \frac{H(t, u) \sinh(t)}{\sqrt{\cosh(t) - \cosh(b)} [\cosh(t) - \cosh(s)]} \times \frac{dt}{\pi^2}. \quad (\text{A10})$$

Using equation (A8), one can simplify equation (A10) into

$$A(s, u) = - \frac{1}{2\pi^2} \int_0^\infty \frac{I_2(t, u) \sinh(t)}{\cosh(t) - \cosh(s)} dt. \quad (\text{A11})$$

One can analytically compute the integration over the variable t in equation (A11). The result leads to equation (35).

Laboratoire de Physique Statistique de l'École Normale Supérieure
24 rue Lhomond
F-75231 Paris Cedex 05, France
(M.A.)

Laboratoire de Géologie de l'École Normale Supérieure
24 rue Lhomond
F-75231 Paris Cedex 05, France
(R.M.)